NANO LETTERS
Letter
Cite This: Nano Lett. 2019, 19, 1527−1533
pubs.acs.org/NanoLett

Isotope Effect in Bilayer WSe_2

Wei Wu,[†,‡] Mayra Daniela Morales-Acosta,[‡] Yongqiang Wang,[§,∥] and Michael Thompson Pettes*[,†,‡,∥]

[†]Department of Mechanical Engineering, University of Connecticut, Storrs, Connecticut 06269, United States
[‡]Institute of Materials Science, University of Connecticut, Storrs, Connecticut 06269, United States
[§]Materials Science and Technology Division, Los Alamos National Laboratory, Los Alamos, New Mexico 87545, United States
[∥]Center for Integrated Nanotechnologies (CINT), Materials Physics and Applications Division, Los Alamos National Laboratory, Los Alamos, New Mexico 87545, United States

Supporting Information

ABSTRACT: Isotopes of an element have the same electron number but differ in neutron number and atomic mass. However, due to the thickness-dependent properties in MX_2 (M = Mo, W; X = S, Se, Te) transition metal dichalcogenides (TMDs), the isotopic effect in atomically thin TMDs still remains unclear especially for phonon-assisted indirect excitonic transitions. Here, we report the first observation of the isotope effect on the electronic and vibrational properties of a TMD material, using naturally abundant $^{NA}W^{NA}Se_2$ and isotopically pure $^{186}W^{80}Se_2$ bilayer single crystals over a temperature range of 4.4−300 K. We demonstrate a higher optical band gap energy in $^{186}W^{80}Se_2$ than in $^{NA}W^{NA}Se_2$ (3.9 ± 0.7 meV from 4.41 to 300 K), which is surprising as isotopes are neutral impurities. Phonon energies decrease in the isotopically pure crystal due to the atomic mass dependence of harmonic oscillations, with correspondingly longer E_{2g} and A^2_{1g} phonon lifetimes than in the naturally abundant sample. The change in electronic band gap renormalization energy is postulated as being the dominant mechanism responsible for the change in optical emission spectra.

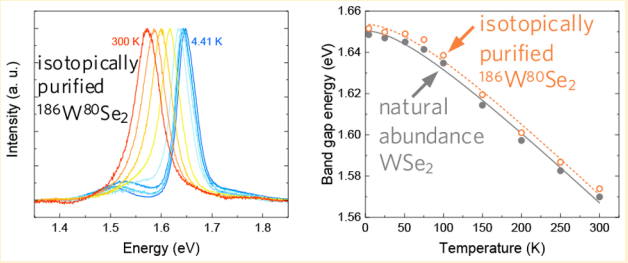

KEYWORDS: *Isotope engineering, band gap engineering, tungsten diselenide, transition metal dichalcogenide, photoluminescence, Raman*

With the discovery of graphene,[1] the atomically thin family of materials receive interest continuously. A wide application in electronics,[2−5] optoelectronics,[6−11] and quantum phononics[12−16] has been achieved with the expansion of this class of materials to the MX_2 (M = Mo, W; X = S, Se, Te) transition metal dichalcogenides (TMDs) possessing large band gaps compared with zero-gap graphene. TMDs are a group of materials consisting of three atom-thick layers with transition metals covalently bonded with chalcogens in trigonal prismatic coordination geometry and adjacent layers bonded by relatively weak van der Waals interactions. Compared to bulk materials, atomically thin TMDs offer size and tunability advantages over traditional materials for miniaturization of electronic and optical devices,[6,7,17] especially as their optoelectronic and vibrational properties are highly dependent on layer thickness.[18,19] Thus, the precise manipulation of electron and phonon band structure in atomically thin TMDs materials is the key to widespread adoption in applications including energy conversion.[20] Reversible modification of the electronic band gap in mono- and bilayer crystals of MoS_2[21] and WSe_2[10,22] has been demonstrated via strain,[23] in which bilayer WSe_2 showed a two-orders of magnitude enhancement of photoluminescence response with uniaxial tensile strain.[10] Another method to extrinsically tune optoelectronic properties has been achieved through application of external electric fields in WSe_2 and $MoSe_2$ monolayers.[11,24] Yet, an intrinsic route to tune the electronic band structure and phonon dispersion relationship in these materials still remains unexplored.

Recently, the tunability of van der Waals interactions and anharmonic phonon scattering in bulk hexagonal boron nitride (*h*-BN) has been proven via experimental observation of changes in the electronic band gap and Raman signature due to the isotope effect.[25,26] However, the isotopic effect on phonon and optoelectronic properties still remains unknown in the TMD class of atomically thin materials. Here, we report isotopic engineering of the optical band gap and phonon energy in atomically thin bilayer naturally abundant $^{NA}W^{NA}Se_2$ and isotopically pure $^{186}W^{80}Se_2$ by combing X-ray diffraction and temperature-dependent Raman and photoluminescence spectroscopy from ∼4 K to room temperature.

WSe_2 occurs naturally with five W isotopes[27] and six Se isotopes[28] with dominant concentrations of ^{184}W (30.64% at.) and ^{80}Se (49.61% at.). The strength of isotopic disorder in a compound is given by the second-order mass variance parameter $g = \sum_{i,j}[c_{i,j}(1-M_{i,j}/M_{i,\mathrm{avg}})^2]$ in transport calculations,[29,30] where $c_{i,j}$ and $M_{i,j}$ are the concentration and atomic

Received: October 23, 2018
Revised: February 12, 2019
Published: February 12, 2019

DOI: 10.1021/acs.nanolett.8b04269
Nano Lett. 2019, 19, 1527−1533

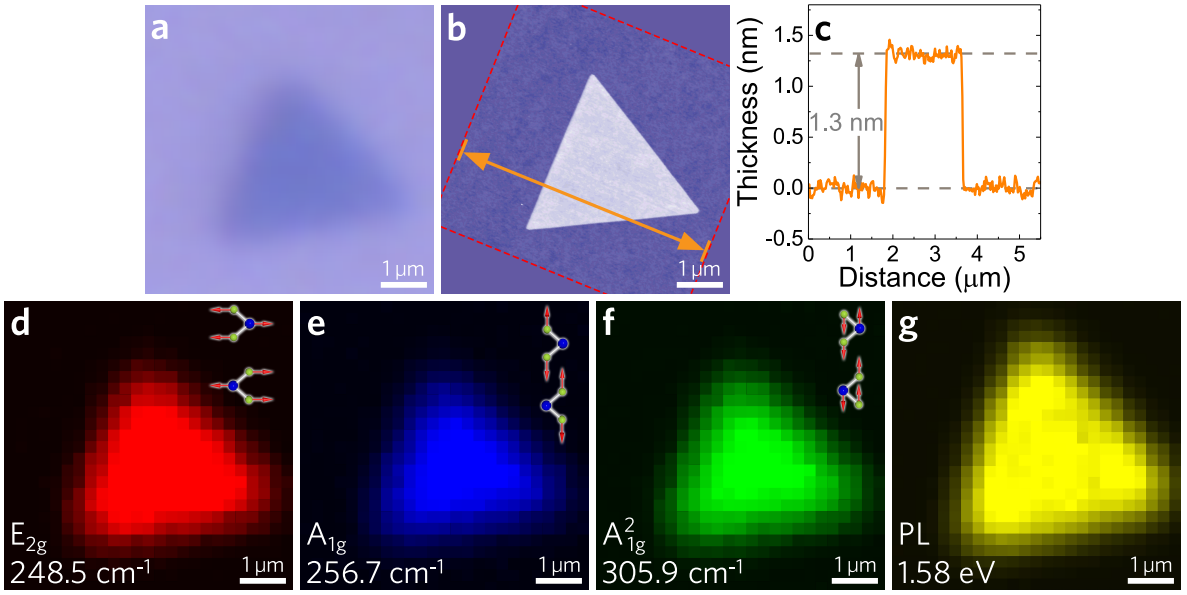

Figure 1. Spatially dependent characterization of an isotopically pure bilayer $^{186}W^{80}Se_2$ crystal. (a) Optical image and (b) atomic force microscopy (AFM) characterization of $^{186}W^{80}Se_2$ on a 285 nm SiO_2-on-Si substrate. (c) AFM height profile corresponding to the line shown in part b. Spatially resolved Raman intensity at (d) 248.5 cm^{-1} (E_{2g} mode), (e) 256.7 cm^{-1} (A_{1g} mode), and (f) 305.9 cm^{-1} (A^2_{1g} mode), where the vibrational modes are depicted schematically. (g) Spatially resolved photoluminescence (PL) intensity at the peak emission wavelength of 1.58 eV.

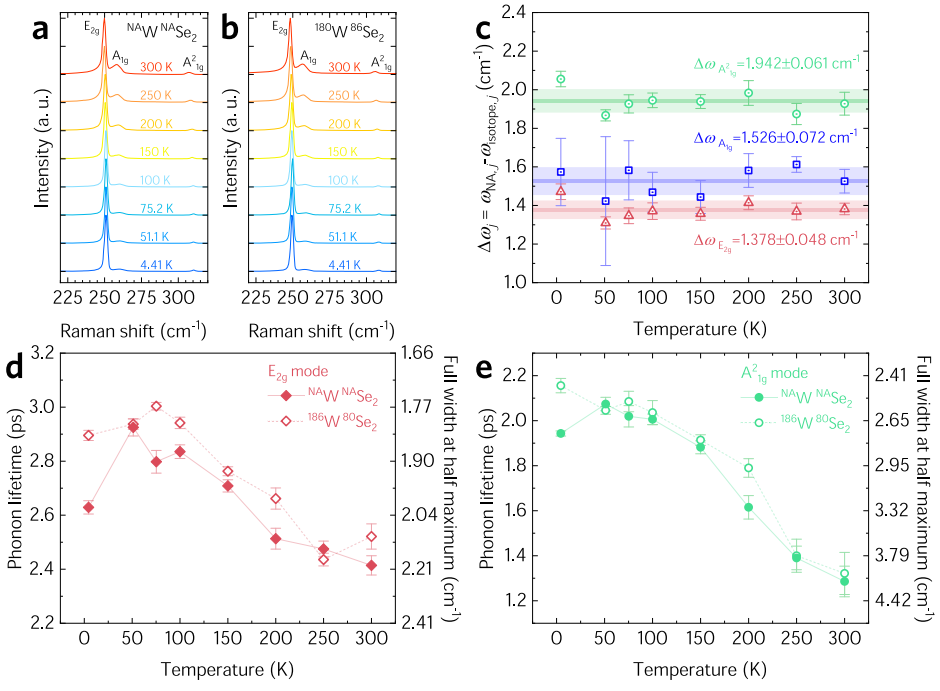

Figure 2. Isotopic mass dependent Raman spectra of bilayer WSe_2. Normalized Raman spectra of (a) naturally abundant $^{NA}W^{NA}Se_2$ and (b) isotopically pure $^{186}W^{80}Se_2$ over the temperature range from 4.41 to 300 K. (c) Phonon frequency difference ($\Delta\omega$) of E_{2g} (red), A_{1g} (blue), and A^2_{1g} (green) modes between $^{NA}W^{NA}Se_2$ and $^{186}W^{80}Se_2$, where error is defined by the standard deviation of six measurements each with a different spectral window initial point in order to account for the instrument uncertainty. Temperature-dependent phonon lifetime and full width at half-maximum of the (d) E_{2g} mode and (e) A^2_{1g} mode from 4.41 to 300 K.

mass of ith atom and the jth impurity, respectively, and $M_{i,avg}$ is the average atomic mass. Naturally occurring $^{NA}W^{NA}Se_2$ has a molecular mass of 341.98u and g of 9.94×10^{-4}, where u is the unified atomic mass constant. The g value can be reduced by more than 377 times to 2.63×10^{-6} with a molecular mass of 345.99u through isotopic purification using ^{186}W and ^{80}Se at commercially available purification levels greater than 99.9% at., indicating that isotopic effects may play an important role in TMDs such as WSe_2 since the natural system is intrinsically disordered.

In this first work on the isotope effect in a TMD material, both naturally abundant $^{NA}W^{NA}Se_2$ and isotopically pure $^{186}W^{80}Se_2$ bilayers were grown by chemical vapor deposition (CVD) on ~285 nm SiO_2-coated silicon substrates similar to our previous report.[10] Since the optical band gap is extremely sensitive to strain and crystalline quality,[10,31,32] the $^{NA}W^{NA}Se_2$

DOI: 10.1021/acs.nanolett.8b04269
Nano Lett. 2019, 19, 1527−1533

and $^{186}W^{80}Se_2$ bilayers are synthesized under identical growth conditions (for details, see methods and the Supporting Information), eliminating differences in structure caused by thermal expansion mismatch with the substrate.[33] To isolate the isotopic effect from the layer number[19,34] and edge effect[35] contributions to the optical band gap, Figure 1a–c demonstrates our bilayer WSe_2 single crystals are synthesized so that the top and bottom layers have the same lateral dimensions. Atomic force microscopy (AFM) analysis shows a uniform thickness of ∼1.3 nm over the entire crystallite for both $^{NA}W^{NA}Se_2$ and $^{186}W^{80}Se_2$ bilayers. Figure 1d–f illustrates that the Raman spectra of an isotopically pure bilayer $^{186}W^{80}Se_2$ crystallite is spatially uniform in intensity throughout the entire crystallite for the E_{2g}, A_{1g}, and A^2_{1g} Raman active modes, which is similar as our previous reported naturally abundant bilayer $^{NA}W^{NA}Se_2$.[10] Photoluminescence (PL) also demonstrates spatially uniform peak intensity and in the entire crystallite (Figure 1g), further indicating the uniformity of atomic-level thickness. Room temperature X-ray diffraction (XRD) analysis of $^{NA}W^{NA}Se_2$ and $^{186}W^{80}Se_2$ is shown in Figure S1 of the Supporting Information. We have also conducted Rutherford backscattering spectrometry (RBS) analysis to obtain the elemental atomic ratios of the materials in this report. Analyzing the scattering yield ratios between W and Se, we obtain a W/Se ratio of 1:1.98 for both the naturally abundant and isotopically enriched samples indicating comparable stoichiometry and hence sample quality (Figure S2, Supporting Information).

Atomic vibrations described as phonons have energies which are dependent on the atomic mass, where frequency changes stemming from isotopic substitution can be monitored by Raman spectroscopy.[36] Figure 2a,b shows the evolution of optical phonon energies with temperature in $^{NA}W^{NA}Se_2$ and $^{186}W^{80}Se_2$ bilayers using Raman spectroscopy and 532 nm laser excitation with a point-to-point resolution of ∼0.51 cm^{-1} using an 1800 gr/mm grating. To minimize the instrumental uncertainty, we conducted six sets of measurements with spectral windows defined by initial points differing by 0.1 cm^{-1} to fully cover the point-to-point separation. The mean and standard deviation of modeled peak positions and full width at half-maximum (fwhm) obtained for each of these six spectra was used as the uncertainty for each data point. To avoid any influence from the slightly nonuniform temperature distribution on the sample mount in the optical cryostat, all Raman spectra were aligned using the silicon substrate peak at each nominal temperature.

The frequency of optical lattice vibrations is expected to decrease with heavier isotopic atomic mass according to a simple one-dimensional harmonic oscillator model[37] as $\omega = [2C\cdot\Sigma_j M_j^{-1}]^{1/2}$ for zone center and $\omega = (2C/M_j)^{1/2}$, j = 1,2, for zone boundary phonons where C is the force constant and M_j is the mass of the jth atom in the two-atom basis chain. The experimental frequency difference between $^{NA}W^{NA}Se_2$ and $^{186}W^{80}Se_2$ bilayers for each Raman active mode is evaluated as $\Delta\omega_i = \omega_{i,NA} - \omega_{i,isotope}$, $i = E_{2g}, A_{1g}, A^2_{1g}$, where ω_i is the Raman peak frequency of the ith Raman active mode. Figure 2c shows that the phonon frequency globally red-shifts in the isotopic samples over the entire temperature range from 4.41 to 300 K. The E_{2g} mode corresponds to intralayer tungsten and selenium atoms vibrating against each other in the hexagonal basal plane, in which the phonon frequency difference between $^{NA}W^{NA}Se_2$ and $^{186}W^{80}Se_2$ bilayers is $\Delta\omega_{E2g}$ = 1.38 ± 0.05 cm^{-1}. The A_{1g} mode represents selenium atom vibrations along the out-of-plane direction with $\Delta\omega_{A1g}$ = 1.53 ± 0.07 cm^{-1}. The more interesting mode here is A^2_{1g} with $\Delta\omega_{A21g}$ = 1.94 ± 0.06 cm^{-1}. The A^2_{1g} mode represents an interlayer vibration involving both tungsten and selenium atoms from different van der Waals layers and only appears for two or more layers of WSe_2.[38] We observe that the isotopic effect on the interlayer out-of-plane A^2_{1g} mode is larger than on the in-plane E_{2g} mode or the intralayer out-of-plane A_{1g} mode, which arises from the fact that the isotopic effect on the weak interlayer van der Waals interaction is slightly larger than it is on the strong intralayer W–Se covalent interaction.

Besides the harmonic oscillation of phonons, the contribution of van der Waals bond length on phonon frequency also needs to be evaluated to support the statement above. The phonon frequency changes due to strain can be defined as[10] $\Delta\omega_{i,strain} = -\varepsilon\gamma_i\omega_i$ where γ is the Grüneisen parameter, ε is the hydrostatic strain, and i represents the phonon mode. The interlayer van der Waals bond length change can be treated as $\Delta c = \varepsilon_{zz}c$, where Δc is the c-lattice parameter change due to isotopic substitution, c is the natural abundance c-lattice parameter, and ε_{zz} is the out-of-plane strain component. Thus, the phonon frequency change due to isotopic substitution in this work can be approximated as $\Delta\omega_{i,strain} = -\gamma_i\omega_i\Delta c/c$. By adopting the experimental Grüneisen parameter of the A^2_{1g} mode in bilayer WSe_2 as 0.357[10] and the c-lattice parameters obtained from XRD analysis, the phonon frequency changes expected due to isotope induced changes in van der Waals bond length can be estimated on the order of $\Delta\omega_{A21g,strain}$ = 0.04 cm^{-1}, which is negligible compared to the measured experimental frequency changes.

The phonon lifetime is an important parameter that describes phonon scattering processes and can be estimated from the fwhm of the Raman peak as[26] $\tau = \hbar/\Gamma$ where τ is the phonon lifetime, $\hbar$ is the reduced Planck constant, and Γ is the fwhm. Figure 2d,e illustrates that isotopically pure $^{186}W^{80}Se_2$ exhibits slightly longer phonon lifetimes for both the intralayer in-plane E_{2g} mode and the interlayer out-of-plane A^2_{1g} mode, although this is still only marginally higher than experimental uncertainty. The observed decrease of the phonon lifetime with temperature arises from an increase of phonon occupancy and phonon–phonon interaction with temperature.[39] At 4.41 (300) K, the phonon lifetime of the E_{2g} mode in bilayer $^{186}W^{80}Se_2$ is 2.90 ± 0.02 (2.52 ± 0.05) ps and ∼2.16 ± 0.03 (1.32 ± 0.09) ps for the A^2_{1g} mode, which is 10.1 (4.42) % and 11.1 (2.77) % higher than the lifetimes of E_{2g} and A_{1g} modes in bilayer $^{NA}W^{NA}Se_2$, respectively.

Figure 3 shows the temperature dependent Raman shift of the E_{2g}, A_{1g}, and A^2_{1g} modes of bilayer $^{NA}W^{NA}Se_2$ and $^{186}W^{80}Se_2$. As the temperature increases from 4.41 to 300 K, the E_{2g} mode frequency decreases by 1.31 ± 0.03 cm^{-1} in $^{NA}W^{NA}Se_2$ and by and 1.22 ± 0.03 cm^{-1} in $^{186}W^{80}Se_2$. The A_{1g} mode frequency drops a similar amount over the same temperature range, 1.58 ± 0.11 cm^{-1} and 1.53 ± 0.06 cm^{-1} in $^{NA}W^{NA}Se_2$ and $^{186}W^{80}Se_2$, respectively. The A^2_{1g} mode frequency drops by nearly twice as much, 2.58 ± 0.03 cm^{-1} and 2.45 ± 0.04 cm^{-1} in $^{NA}W^{NA}Se_2$ and $^{186}W^{80}Se_2$ bilayers, respectively. This behavior can be explained by the positive thermal expansion coefficient (TEC) of both in-plane and out-of-plane unit cell parameters.[40,41] We observe that the out-of-plane vibrational modes, A_{1g} and A^2_{1g}, have ∼1.2 and ∼1.9 times higher frequency changes than the in-plane vibration

DOI: 10.1021/acs.nanolett.8b04269
Nano Lett. 2019, 19, 1527–1533

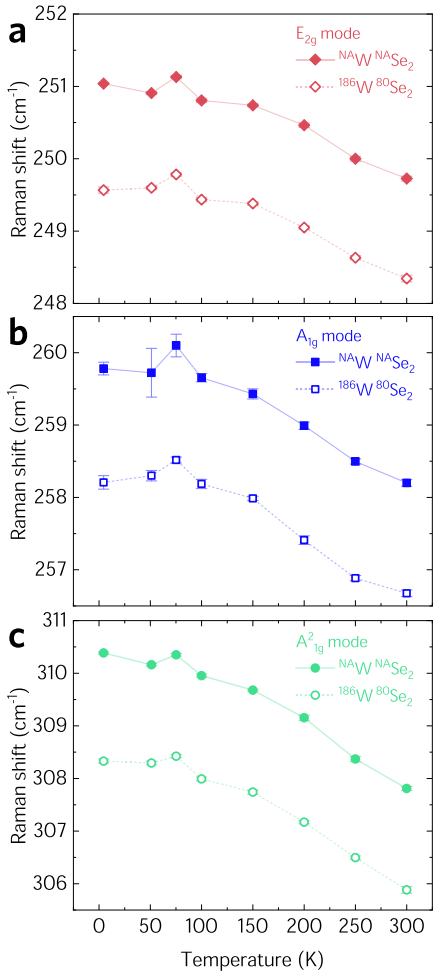

Figure 3. Temperature dependence of Raman active mode peak positions in isotopically engineered bilayer WSe_2. Raman shift for the (a) E_{2g}, (b) A_{1g}, and (c) A^2_{1g} modes of naturally abundant $^{NA}W^{NA}Se_2$ (solid symbols) and isotopically pure $^{186}W^{80}Se_2$ (open symbols).

mode (E_{2g}), respectively, which arises from an out-of-plane TEC approximately 1.6 times higher than the in-plane TEC.[41]

Electronic transitions from filled to empty states must conserve electron momentum. Bilayer WSe_2 is known as a semiconductor with an indirect electronic band gap,[19] in which the conduction band minimum at the Σ-point (CBM_Σ) and valence band maximum at the K-point (VBM_K) are not at the same electron momentum in reciprocal space. Since the momentum of photons is negligible, especially in the wavelength range used in this work, the transition between CBM_Σ and VBM_K must involve phonon assistance to obey the rule of momentum conservation, which means the band gap can be affected by the isotope effect. Furthermore, phonon energy tuning by the isotope effect may also result from a change in wave vector arising from a shift of the PL band gap energy. Figure 4 reports the temperature dependent PL spectra for bilayer $^{NA}W^{NA}Se_2$ and $^{186}W^{80}Se_2$. To avoid uncertainty arising from nonidentical local heating by the excitation laser, all the samples were characterized under the same conditions including laser power and acquisition time at each temperature. Surprisingly, we observe a higher optical band gap energy in bilayer $^{186}W^{80}Se_2$ compared with bilayer $^{NA}W^{NA}Se_2$ where the PL spectra of the isotopically pure sample blue-shifts by 3.9 ± 0.7 meV over the entire temperature range from 4.41 to 300 K (Figure 4c). This trend is similar to the PL spectra blue-shift with increasing atomic mass phenomenon observed in other isotopically purified indirect band gap semiconductors, where the indirect band gap renormalization energy changes ∼4.4 meV between h-^{10}BN and h-^{NA}BN,[25] and ∼2.2 meV between ^{70}Ge and ^{76}Ge.[42]

The mechanisms responsible for this observable change in emission energy are indirect band gap renormalization[43] and isotopic phonon energy shift.[25] When evaluating the normalized electronic states in an indirect band gap semiconductor, the band gap renormalization energy is inversely proportional to the square root of effective mass and depends on the zero-point vibrational energy, calculated with all phonon modes at zero temperature. The isotope effect on indirect band gap renormalization energy has been proven in bulk h-BN.[25] However, the phonon replicas of MX_2 TMDs can only be obtained by resonant Raman spectroscopy, rather than the nonresonant spectra which is used here and in the previous h-BN report.[25] Another approach to estimate the renormalization energy is to extrapolate the linear relationship between temperature and band gap energy at high temperature, which is up to 800 K for bulk h-BN[25] and 1000 K for Ge.[43] Comparing to h-BN, the atomically thin MX_2 TMDs are extremely sensitive to oxygen,[44] so there has been no available report of the PL spectra above 400 K of atomically thin WSe_2. The band gap renormalization energy is proportional to $\mu^{-1/2}$, and thus can be calculated as $\delta E_g^{\alpha} = \delta E_g^{NA}(\mu^{\alpha}/\mu^{NA})^{1/2}$, where α represents the isotope and μ indicates the reduced mass. Since both bilayer WSe_2 and WS_2 are indirect semiconductors, sharing the same lamellar structure and having similar band gaps, we adopt the experimental band gap renormalization energy of bilayer WS_2 bilayer for bilayer $^{NA}W^{NA}Se_2$, $\delta E_g^{NA} \sim$ 500 meV.[45] The change of band gap renormalization energy in the isotopically enriched sample can then be estimated as $\delta E_g^{\alpha} - \delta E_g^{NA} \approx 2.99$ meV. Therefore, the isotopic band gap renormalization dominates the PL band gap shift which is measured as 3.9 ± 0.7 meV in this study.

It is also important to evaluate the contribution of van der Waals bond length change to optical band gap energy, as out-of-plane compressive strain has been shown to decrease the indirect optical band gap energy in bilayer WSe_2.[10] A similar trend has also been predicted for bilayer MoS_2, in which the indirect band gap decreases with shorter c-lattice parameter.[46] This is contrary to our observation of the higher optical band gap in bilayer $^{186}W^{80}Se_2$ which possesses a smaller c-lattice parameter than $^{NA}W^{NA}Se_2$. Therefore, we conclude that the van der Waals bond length is not the dominant factor resulting in the optical band gap energy change with isotopic purification in this work. The temperature evolution of the optical band gap is shown in Figure 4d, which decreases from 1.649 eV at 4.41 K to 1.599 eV at 300 K for $^{NA}W^{NA}Se_2$ and from 1.652 eV at 4.41 K to 1.574 eV at 300 K for $^{186}W^{80}Se_2$. This behavior can be modeled using the empirical Varshni relation[47] as $E_g(T) = E_g(T=0) - (\alpha T^2)/(\beta + T)$ where $E_g(T=0)$ is the band gap energy at 0 K, T is the absolute temperature, and α and β are adjustable constants. We obtained $E_g(T=0) = 1.650$ eV, $\alpha = 0.365$ meV/K, and $\beta = 93.93$ K for $^{NA}W^{NA}Se_2$, and $E_g(T=0) = 1.654$ eV, $\alpha = 0.379$ meV/K, and $\beta = 112.96$ K for $^{186}W^{80}Se_2$. Coefficients of determination were 0.991 and 0.992 for $^{NA}W^{NA}Se_2$ and $^{186}W^{80}Se_2$, respectively. The slight difference between our experimental data and the empirical modeling at low temperature arises from the quadratic temperature dependence

DOI: 10.1021/acs.nanolett.8b04269
Nano Lett. 2019, 19, 1527−1533

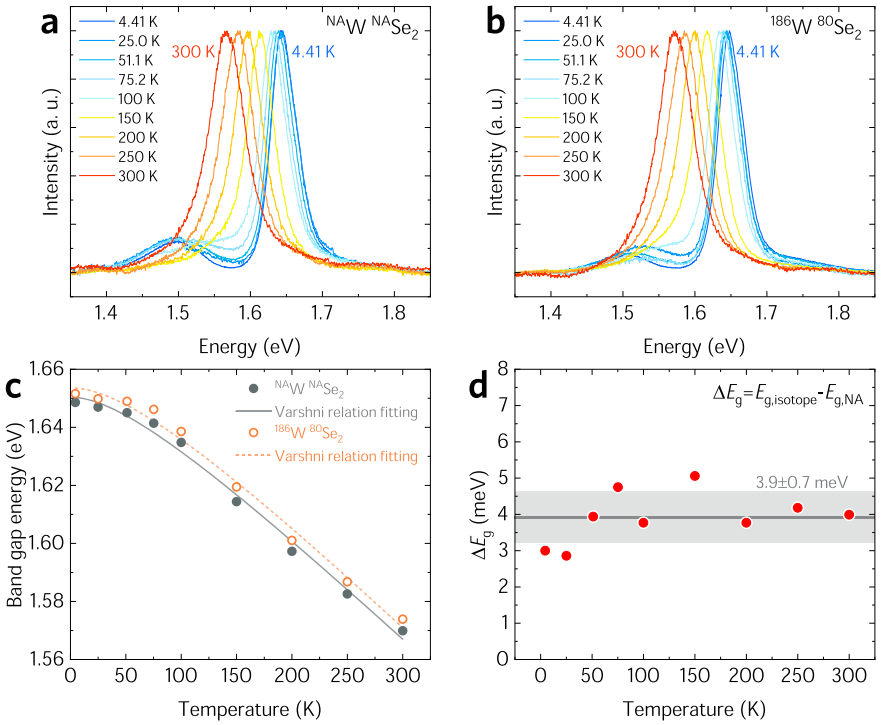

Figure 4. Isotopic mass dependent photoluminescence and optical band gap. Normalized photoluminescence spectra over a temperature range from 4.41 to 300 K for (a) naturally abundant bilayer $^{NA}W^{NA}Se_2$ and (b) isotopically pure bilayer $^{186}W^{80}Se_2$. (c) Temperature dependence of the band gap of $^{NA}W^{NA}Se_2$ and $^{186}W^{80}Se_2$, where modeling results using the empirical Varshni relation are given by solid and dashed lines, respectively. (d) Difference in optical band gap between $^{NA}W^{NA}Se_2$ and $^{186}W^{80}Se_2$ as a function of temperature.

of the empirical Varshni relation, whereas theoretical and experimental observations are reported to exhibit T^4 dependence at low temperature.[43,48,49]

In conclusion, we have experimentally demonstrated the isotope effect on the phonon frequency, phonon lifetime, and optical band gap energy in an atomically thin TMD through temperature dependent spectroscopy of naturally abundant and isotopically pure bilayer WSe_2. We have postulated a new mechanism by which the electronic band gap energy and phonon dispersion can be tuned in this material by isotopic enrichment. The outcomes of this study should help stimulate future investigations and theoretical predictions of phonon and electronic property modification in other isotopically enriched van der Waals material systems, such as the isotope effect on thermal conductivity.[36,50−53]

■ ASSOCIATED CONTENT

Supporting Information

The Supporting Information is available free of charge on the ACS Publications website at DOI: 10.1021/acs.nanolett.8b04269.

Additional synthesis, structural characterization, and experimental details (PDF)

■ AUTHOR INFORMATION

Corresponding Author

*E-mail: pettesmt@lanl.gov.

ORCID

Michael Thompson Pettes: 0000-0001-6862-6841

Author Contributions

This project was conceived and led by M.T.P.; W.W. and M.T.P. conducted WSe_2 synthesis, experimental characterizations, and analytical modeling; W.W. and M.D.M.-A. performed X-ray diffraction spectroscopy and analysis. The manuscript was written by M.T.P. and W.W. with contributions from all authors.

Notes

The authors declare no competing financial interest.

■ ACKNOWLEDGMENTS

This work was supported by the U.S. National Science Foundation under Award No. CAREER-1553987 (M.T.P., W.W.). This work was performed, in part, at the Center for Integrated Nanotechnologies, an Office of Science User Facility operated for the U.S. Department of Energy (DOE) Office of Science. Los Alamos National Laboratory, an affirmative action equal opportunity employer, is managed by Triad National Security, LLC for the U.S. Department of Energy's NNSA, under Contract 89233218CNA000001. This work was performed, in part, at the Harvard University Center for Nanoscale Systems (CNS), a member of the National Nanotechnology Coordinated Infrastructure Network (NNCI), which is supported by the U.S. National Science Foundation under Award No. 1541959.

■ REFERENCES

(1) Novoselov, K. S.; Geim, A. K.; Morozov, S. V.; Jiang, D.; Zhang, Y.; Dubonos, S. V.; Grigorieva, I. V.; Firsov, A. A. Electric field effect in atomically thin carbon films. *Science* **2004**, *306*, 666−669.

(2) Geim, A. K.; Grigorieva, I. V. Van der Waals heterostructures. *Nature* **2013**, *499*, 419−425.

(3) Chhowalla, M.; Shin, H. S.; Eda, G.; Li, L.-J.; Loh, K. P.; Zhang, H. The chemistry of two-dimensional layered transition metal dichalcogenide nanosheets. *Nat. Chem.* **2013**, *5*, 263−275.

DOI: 10.1021/acs.nanolett.8b04269
Nano Lett. 2019, 19, 1527−1533

(4) Bhimanapati, G. R.; Lin, Z.; Meunier, V.; Jung, Y.; Cha, J.; Das, S.; Xiao, D.; Son, Y.; Strano, M. S.; Cooper, V. R.; Liang, L.; Louie, S. G.; Ringe, E.; Zhou, W.; Kim, S. S.; Naik, R. R.; Sumpter, B. G.; Terrones, H.; Xia, F.; Wang, Y.; Zhu, J.; Akinwande, D.; Alem, N.; Schuller, J. A.; Schaak, R. E.; Terrones, M.; Robinson, J. A. Recent advances in two-dimensional materials beyond graphene. *ACS Nano* **2015**, *9*, 11509−11539.
(5) Zhou, H.; Wang, C.; Shaw, J. C.; Cheng, R.; Chen, Y.; Huang, X.; Liu, Y.; Weiss, N. O.; Lin, Z.; Huang, Y.; Duan, X. Large area growth and electrical properties of p-type WSe_2 atomic layers. *Nano Lett.* **2015**, *15*, 709−713.
(6) Mak, K. F.; Shan, J. Photonics and optoelectronics of 2D semiconductor transition metal dichalcogenides. *Nat. Photonics* **2016**, *10*, 216−226.
(7) Schaibley, J. R.; Yu, H.; Clark, G.; Rivera, P.; Ross, J. S.; Seyler, K. L.; Yao, W.; Xu, X. Valleytronics in 2D materials. *Nat. Rev. Mater.* **2016**, *1*, 16055.
(8) Lee, C.-H.; Lee, G.-H.; van der Zande, A. M.; Chen, W.; Li, Y.; Han, M.; Cui, X.; Arefe, G.; Nuckolls, C.; Heinz, T. F.; Guo, J.; Hone, J.; Kim, P. Atomically thin p−n junctions with van der Waals heterointerfaces. *Nat. Nanotechnol.* **2014**, *9*, 676−681.
(9) Huang, C.; Wu, S.; Sanchez, A. M.; Peters, J. J. P.; Beanland, R.; Ross, J. S.; Rivera, P.; Yao, W.; Cobden, D. H.; Xu, X. Lateral heterojunctions within monolayer $MoSe_2$−WSe_2 semiconductors. *Nat. Mater.* **2014**, *13*, 1096−1101.
(10) Wu, W.; Wang, J.; Ercius, P.; Wright, N. C.; Leppert-Simenauer, D. M.; Burke, R. A.; Dubey, M.; Dongare, A. M.; Pettes, M. T. Giant mechano-optoelectronic effect in an atomically thin semiconductor. *Nano Lett.* **2018**, *18*, 2351−2357.
(11) Chakraborty, C.; Kinnischtzke, L.; Goodfellow, K. M.; Beams, R.; Vamivakas, A. N. Voltage-controlled quantum light from an atomically thin semiconductor. *Nat. Nanotechnol.* **2015**, *10*, 507−511.
(12) Tonndorf, P.; Schmidt, R.; Schneider, R.; Kern, J.; Buscema, M.; Steele, G. A.; Castellanos-Gomez, A.; van der Zant, H. S. J.; Michaelis de Vasconcellos, S.; Bratschitsch, R. Single-photon emission from localized excitons in an atomically thin semiconductor. *Optica* **2015**, *2*, 347−352.
(13) Palacios-Berraquero, C.; Barbone, M.; Kara, D. M.; Chen, X.; Goykhman, I.; Yoon, D.; Ott, A. K.; Beitner, J.; Watanabe, K.; Taniguchi, T.; Ferrari, A. C.; Atatüre, M. Atomically thin quantum light-emitting diodes. *Nat. Commun.* **2016**, *7*, 12978.
(14) Branny, A.; Kumar, S.; Proux, R.; Gerardot, B. D. Deterministic strain-induced arrays of quantum emitters in a two-dimensional semiconductor. *Nat. Commun.* **2017**, *8*, 15053.
(15) Palacios-Berraquero, C.; Kara, D. M.; Montblanch, A. R. P.; Barbone, M.; Latawiec, P.; Yoon, D.; Ott, A. K.; Loncar, M.; Ferrari, A. C.; Atatüre, M. Large-scale quantum-emitter arrays in atomically thin semiconductors. *Nat. Commun.* **2017**, *8*, 15093.
(16) He, Y.-M.; Clark, G.; Schaibley, J. R.; He, Y.; Chen, M.-C.; Wei, Y.-J.; Ding, X.; Zhang, Q.; Yao, W.; Xu, X.; Lu, C.-Y.; Pan, J.-W. Single quantum emitters in monolayer semiconductors. *Nat. Nanotechnol.* **2015**, *10*, 497−502.
(17) Iannaccone, G.; Bonaccorso, F.; Colombo, L.; Fiori, G. Quantum engineering of transistors based on 2D materials heterostructures. *Nat. Nanotechnol.* **2018**, *13*, 183−191.
(18) Mak, K. F.; Lee, C.; Hone, J.; Shan, J.; Heinz, T. F. Atomically thin MoS_2: A new direct-gap semiconductor. *Phys. Rev. Lett.* **2010**, *105*, 136805.
(19) Zhao, W.; Ghorannevis, Z.; Chu, L.; Toh, M.; Kloc, C.; Tan, P.-H.; Eda, G. Evolution of electronic structure in atomically thin sheets of WS_2 and WSe_2. *ACS Nano* **2013**, *7*, 791−797.
(20) Yazdani, S.; Pettes, M. T. Nanoscale self-assembly of thermoelectric materials: A review of chemistry-based approaches. *Nanotechnology* **2018**, *29*, 432001.
(21) Conley, H. J.; Wang, B.; Ziegler, J. I.; Haglund, R. F.; Pantelides, S. T.; Bolotin, K. I. Bandgap engineering of strained monolayer and bilayer MoS_2. *Nano Lett.* **2013**, *13*, 3626−3630.
(22) Desai, S. B.; Seol, G.; Kang, J. S.; Fang, H.; Battaglia, C.; Kapadia, R.; Ager, J. W.; Guo, J.; Javey, A. Strain-induced indirect to direct bandgap transition in multilayer WSe_2. *Nano Lett.* **2014**, *14*, 4592−4597.
(23) Dai, Z.; Liu, L.; Zhang, Z. Strain engineering of 2D materials: Issues and opportunities at the interface. *Adv. Mater.* **2019**, 1805417.
(24) He, K.; Poole, C.; Mak, K. F.; Shan, J. Experimental demonstration of continuous electronic structure tuning via strain in atomically thin MoS_2. *Nano Lett.* **2013**, *13*, 2931−2936.
(25) Vuong, T. Q. P.; Liu, S.; Van der Lee, A.; Cuscó, R.; Artús, L.; Michel, T.; Valvin, P.; Edgar, J. H.; Cassabois, G.; Gil, B. Isotope engineering of van der Waals interactions in hexagonal boron nitride. *Nat. Mater.* **2017**, *17*, 152−158.
(26) Cuscó, R.; Artús, L.; Edgar, J. H.; Liu, S.; Cassabois, G.; Gil, B. Isotopic effects on phonon anharmonicity in layered van der Waals crystals: Isotopically pure hexagonal boron nitride. *Phys. Rev. B: Condens. Matter Mater. Phys.* **2018**, *97*, 155435.
(27) Völkening, J.; Köppe, M.; Heumann, K. G. Tungsten isotope ratio determinations by negative thermal ionization mass spectrometry. *Int. J. Mass Spectrom. Ion Processes* **1991**, *107*, 361−368.
(28) Wachsmann, M.; Heumann, K. G. Negative thermal ionization mass spectroscopy of main group elements Part 2. 6th group: Sulfur, selenium and tellurium. *Int. J. Mass Spectrom. Ion Processes* **1992**, *114*, 209−220.
(29) Klemens, P. G. The scattering of low-frequency lattice waves by static imperfections. *Proc. Phys. Soc., London, Sect. A* **1955**, *68*, 1113−1128.
(30) Tamura, S. Isotope scattering of dispersive phonons in Ge. *Phys. Rev. B: Condens. Matter Mater. Phys.* **1983**, *27*, 858−866.
(31) Schmidt, R.; Niehues, I.; Schneider, R.; Drüppel, M.; Deilmann, T.; Rohlfing, M.; Michaelis de Vasconcellos, S.; Castellanos-Gomez, A.; Bratschitsch, R. Reversible uniaxial strain tuning in atomically thin WSe_2. *2D Mater.* **2016**, *3*, 021011.
(32) Liu, Z.; Amani, M.; Najmaei, S.; Xu, Q.; Zou, X.; Zhou, W.; Yu, T.; Qiu, C.; Birdwell, A. G.; Crowne, F. J.; Vajtai, R.; Yakobson, B. I.; Xia, Z.; Dubey, M.; Ajayan, P. M.; Lou, J. Strain and structure heterogeneity in MoS_2 atomic layers grown by chemical vapour deposition. *Nat. Commun.* **2014**, *5*, 5246.
(33) Ahn, G. H.; Amani, M.; Rasool, H.; Lien, D.-H.; Mastandrea, J. P.; Ager, J. W., III; Dubey, M.; Chrzan, D. C.; Minor, A. M.; Javey, A. Strain-engineered growth of two-dimensional materials. *Nat. Commun.* **2017**, *8*, 608.
(34) Tonndorf, P.; Schmidt, R.; Böttger, P.; Zhang, X.; Börner, J.; Liebig, A.; Albrecht, M.; Kloc, C.; Gordan, O.; Zahn, D. R. T.; Michaelis de Vasconcellos, S.; Bratschitsch, R. Photoluminescence emission and Raman response of monolayer MoS_2, $MoSe_2$, and WSe_2. *Opt. Express* **2013**, *21*, 4908−4916.
(35) Dong, L.; Wang, J.; Namburu, R.; O'Regan, T. P.; Dubey, M.; Dongare, A. M. Edge effects on band gap energy in bilayer 2H-MoS_2 under uniaxial strain. *J. Appl. Phys.* **2015**, *117*, 244303.
(36) Pettes, M. T.; Ji, H. X.; Sadeghi, M. M.; Jo, I.; Wu, W.; Ruoff, R. S.; Shi, L. Scattering of phonons by high-concentration isotopic impurities in ultrathin graphite. *Phys. Rev. B: Condens. Matter Mater. Phys.* **2015**, *91*, 035429.
(37) Kittel, C. *Introduction to Solid State Physics*, 8th ed.; John Wiley & Sons: New York, 2005.
(38) Terrones, H.; Corro, E. D.; Feng, S.; Poumirol, J. M.; Rhodes, D.; Smirnov, D.; Pradhan, N. R.; Lin, Z.; Nguyen, M. A. T.; Elías, A. L.; Mallouk, T. E.; Balicas, L.; Pimenta, M. A.; Terrones, M. New first order Raman-active modes in few layered transition metal dichalcogenides. *Sci. Rep.* **2015**, *4*, 4215.
(39) Beechem, T.; Graham, S. Temperature and doping dependence of phonon lifetimes and decay pathways in GaN. *J. Appl. Phys.* **2008**, *103*, 093507.
(40) Hu, X.; Yasaei, P.; Jokisaari, J.; Ögüt, S.; Salehi-Khojin, A.; Klie, R. F. Mapping thermal expansion coefficients in freestanding 2D materials at the nanometer scale. *Phys. Rev. Lett.* **2018**, *120*, 055902.
(41) Murray, R.; Evans, B. The thermal expansion of 2H-MoS_2 and 2H-WSe_2 between 10 and 320 K. *J. Appl. Crystallogr.* **1979**, *12*, 312−315.

DOI: 10.1021/acs.nanolett.8b04269
Nano Lett. 2019, 19, 1527−1533

(42) Etchegoin, P.; Weber, J.; Cardona, M.; Hansen, W. L.; Itoh, K.; Haller, E. E. Isotope effect in Ge: A photoluminescence study. *Solid State Commun.* **1992**, *83*, 843−848.
(43) Cardona, M.; Thewalt, M. L. W. Isotope effects on the optical spectra of semiconductors. *Rev. Mod. Phys.* **2005**, *77*, 1173−1224.
(44) Kang, K.; Godin, K.; Kim, Y. D.; Fu, S.; Cha, W.; Hone, J.; Yang, E.-H. Graphene-assisted antioxidation of tungsten disulfide monolayers: Substrate and electric-field effect. *Adv. Mater.* **2017**, *29*, 1603898.
(45) Chernikov, A.; Ruppert, C.; Hill, H. M.; Rigosi, A. F.; Heinz, T. F. Population inversion and giant bandgap renormalization in atomically thin WS_2 layers. *Nat. Photonics* **2015**, *9*, 466−470.
(46) Cao, B.; Li, T. Interlayer electronic coupling in arbitrarily stacked MoS_2 bilayers controlled by interlayer S−S interaction. *J. Phys. Chem. C* **2015**, *119*, 1247−1252.
(47) Varshni, Y. P. Temperature dependence of the energy gap in semiconductors. *Physica* **1967**, *34*, 149−154.
(48) Cardona, M.; Kremer, R. K. Temperature dependence of the electronic gaps of semiconductors. *Thin Solid Films* **2014**, *571*, 680−683.
(49) Lautenschlager, P.; Allen, P. B.; Cardona, M. Temperature dependence of band gaps in Si and Ge. *Phys. Rev. B: Condens. Matter Mater. Phys.* **1985**, *31*, 2163−2171.
(50) Wu, X.; Yang, N.; Luo, T. Unusual isotope effect on thermal transport of single layer molybdenum disulphide. *Appl. Phys. Lett.* **2015**, *107*, 191907.
(51) Chen, S.; Wu, Q.; Mishra, C.; Kang, J.; Zhang, H.; Cho, K.; Cai, W.; Balandin, A. A.; Ruoff, R. S. Thermal conductivity of isotopically modified graphene. *Nat. Mater.* **2012**, *11*, 203−207.
(52) Lindsay, L.; Broido, D. A. Enhanced thermal conductivity and isotope effect in single-layer hexagonal boron nitride. *Phys. Rev. B: Condens. Matter Mater. Phys.* **2011**, *84*, 155421.
(53) Li, X.; Zhang, J.; Puretzky, A. A.; Yoshimura, A.; Sang, X.; Cui, Q.; Li, Y.; Liang, L.; Ghosh, A. W.; Zhao, H.; Unocic, R. R.; Meunier, V.; Rouleau, C. M.; Sumpter, B. G.; Geohegan, D. B.; Xiao, K. Isotope-Engineering the Thermal Conductivity of Two-Dimensional MoS_2. *ACS Nano* **2019**, DOI: 10.1021/acsnano.8b09448.

DOI: 10.1021/acs.nanolett.8b04269
Nano Lett. 2019, 19, 1527−1533